Available online at www.sciencedirect.com

SciVerse ScienceDirect

Ceramics International 39 (2013) 7721–7725

CERAMICS INTERNATIONAL

www.elsevier.com/locate/ceramint

One-step synthesis of $Ni_{0.5}Zn_{0.5}Fe_2O_4$ fine-patterned films via photosensitive sol–gel route

Fuxue Yan*, Gaoyang Zhao, Yuanqing Chen, Na Song, Nana Zhao, Caiyin You

School of Materials Science and Engineering, Xi'an University of Technology, Xi'an 710048, PR China

Received 2 February 2013; received in revised form 23 February 2013; accepted 10 March 2013
Available online 16 March 2013

Abstract

$Ni_{1-x}Zn_xFe_2O_4$ (NZFO) ($x=0.0$–0.7) films were prepared by a photosensitive sol–gel route utilizing nickel acetate, zinc acetate and ferric nitrate as starting materials. The saturation magnetization of the NZFO film showed a parabolic tendency with Zn substitution. For Zn substitution of 0.5, the saturation magnetization reached the maximum value of 683 emu/cm^3 with a relative low coercivity of 56 Oe at room temperature. The phase constituents and surface morphology of the films were characterized by X-ray diffractometer (XRD), Raman spectroscopy, X-ray photoelectron spectroscopy (XPS), field emission scanning electron microscopy (FESEM) and transmission electron microscopy (TEM). Through a direct patterning process, a fine-patterned $Ni_{0.5}Zn_{0.5}Fe_2O_4$ film was obtained by a photochemical reaction between the chelated complexes and UV light.

Keywords: A. Films; A. Sol–gel process; C. Magnetic properties; D. Ferrites

1. Introduction

Micro-fabrication technology has attracted much attention in the areas of integrated circuits, quantum devices and high density data storage. In the past decades, scientists have been trying to explore new types of small structures, or downsize the existed structures [1,2]. Fine-patterning process is one of the key procedures for realizing the large-scale integrated circuits. As a traditional and effective lithography technology [3–6], the dry etching process usually requires complex lithographic patterning steps with high cost. In addition, the the dry etching may also degrade the properties of films due to the pollution from hazardous materials, which limits its use for some functional materials such as inorganic films. Meanwhile, some newly-developed techniques, such as the photochemical deposition method and the photosensitive sol–gel method, have been successfully applied to prepare fine patterns [7–10]. Since the photosensitive gel film can behave as the photoresist of itself during the preparation process, it can greatly simplify the lithography process. Moreover, using the photosensitive sol–gel route, the deposition of the patterned superconducting thin film and semiconducting thin film has been realized [11,12]. So far, few literatures have been reported on preparing magnetic ferrite films using this method. It is well known that Ni–Zn ferrite possesses low dielectric losses and tunable magnetic inductions, which make them potential candidates for spintronics or higher-frequency devices [13–16]. Therefore, fine-patterning of Ni–Zn ferrite is of great importance for electro-magnetic devices.

In this work, $Ni_{1-x}Zn_xFe_2O_4$ (Later called NZFO) (x=0.0–0.7) thin films were prepared using photosensitive sol–gel method. The magnetic properties, phase constituents, surface morphology and cross-section morphology of the fired films were characterized. The purpose is to fabricate Ni–Zn ferrite films and film micro-patterns with better magnetic properties.

2. Experimental

Nickel acetate ($Ni(CH_3COO)_2\cdot 4H_2O$), zinc acetate ($(CH_3COO)_2Zn\cdot 2H_2O$) and ferric nitrate ($Fe(NO_3)_3\cdot 9H_2O$) were chosen as the sources for Ni, Zn and Ti ions. They were individually mixed with 2-methoxyethanol (MOE) and acetylacetone (AcAcH) at the molar ratio of M:AcAcH:MOE=1:0.6:40 (M=Ni, Zn and Fe) to make three solutions,

*Corresponding author. Tel.: +86 29 82312530; fax: +86 29 82312782.
E-mail address: yanfuxue@126.com (F.X. Yan).

0272-8842/$ - see front matter © 2013 Elsevier Ltd and Techna Group S.r.l. All rights reserved.
http://dx.doi.org/10.1016/j.ceramint.2013.03.027

namely, the Ni-solution, Zn-solution, and Fe-solution. Subsequently, these precursors were mixed according to the molar ratio of Ni:Zn:Fe=(1−x):x:2 (x=0.0, 0.1, 0.2, 0.3, 0.4, 0.5, 0.6, and 0.7) to obtain a NZFO colloid with the total metallic ion concentration of 0.15 mol/L. After that, the colloid was aged for 24 h. The NZFO gel films were coated on the Si substrates through a dip-coating method. Then, the film was pre-dried at 200 °C for 5 min to remove the residual organic compounds. These processes of the coating–drying were repeated three times. Finally, the pre-dried solutions were held at 400–650 °C for 1 h to obtain the crystallized film.

The fine-patterned of $Ni_{1-x}Zn_xFe_2O_4$ films were fabricated as follows: First, the coated NZFO gel films were dried at 40 °C for 10 min, followed by irradiated under ultraviolet light. Second, the gel films were rinsed in a butyl alcohol solutionto get the patterned gel films. The pattern gel films were finally converted to patterned inorganic films through heat treatment.

The magnetic properties were tested using vibrating sample magnetometer (Versalab, Quantum Design). The phase constituents and crystallinity were characterized by X-ray diffraction using CuKα radiation (XRD-7000, Shimadzu). The Raman measurement was performed in backscattering geometry on a Raman spectroscope (LabRAM HR800, HORIBA Jobin Yvon) with a radiation of Ar^+ laser at 633 nm. The cross-section morphology and the corresponding selected area electron diffraction of the films were performed by transmission electron microscopy (JEM-3010, JEOL). The chemical bonding states were determined by X-ray photoelectron spectroscopy (XPS) (Kratos, Shimadzu). XPS spectra were obtained with monochromatic Al Kα (1486.71 eV) line at a power of 150 W (10 mA, 15 kV). The charge neutralizer was used to compensate for surface charge effects, and the binding energies were calibrated using the C1s hydrocarbon peak at 284.8 eV. The surface morphology of the films was observed by field emission scanning electron microscopy (JSM-7000F, JOEL). The optical absorption of the films was performed on a Fourier transform infrared spectroscopy (IR Prestige-21, Shimadzu) and a UV–vis spectrometer (V-570, Shimadzu). The morphology of the patterned gel films were examined using an optical microscope (BX51 TRF, Olympus).

3. Results and discussion

3.1. Phase constituents, morphology and physical properties

Fig. 1 shows the XRD patterns of the NZFO (x=0) films fired at different temperatures of 400 °C, 500 °C, 550 °C, 600 °C and 650 °C. As seen from Fig. 1, the films began to crystallize at the temperature above 500 °C. With the increase of the firing temperature, the crystallinity of the film was improved. At 650 °C, the film showed a better crystallinity with a cubic spinel structure (ref. JCPDS no.74-2081), and no second phase was presented.

Fig. 2 shows the magnetization versus applied magnetic field for NZFO (x=0.0, 0.1, 0.2, 0.3, 0.4, 0.5, 0.6, and 0.7) thin films (fired at 650 °C) at room temperature. All films showed a soft magnetic characteristic. From the inset shown in Fig. 2, the saturation magnetization (Ms) exhibited a maximum value at x=0.5. Meanwhile, the coercivity (Hc) decreased with the increase of Zn content. For the Zn content of 0.5, the Ms reached the maximum of 683 emu/cm^3 and a relative low Hc value of 56 Oe, in which the value of Ms was higher than the data reported by the literatures [16–19]. Therefore, $Ni_{0.5}Zn_{0.5}Fe_2O_4$ film was selected to prepare fine-patterned Ni–Zn ferrite film.

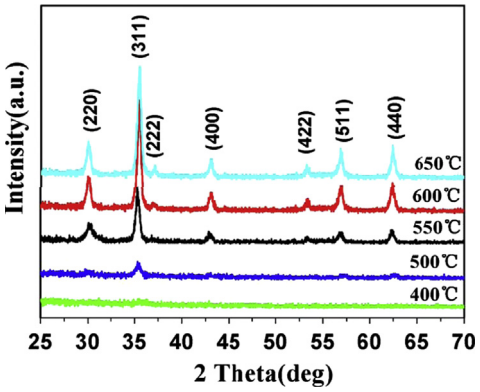

Fig. 1. XRD patterns of NZFO (x=0) films fired at different temperatures.

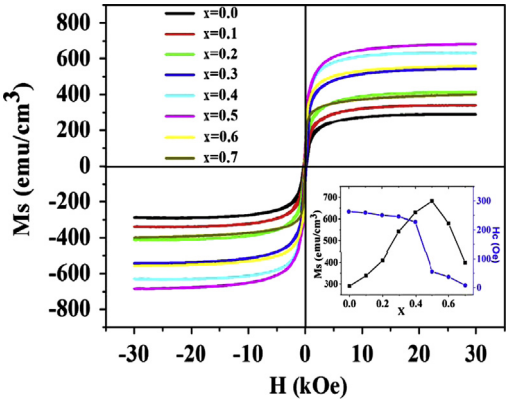

Fig. 2. Magnetic hysteresis loops for NZFO thin films (x=0.0, 0.1, 0.2, 0.3, 0.4, 0.5, 0.6, and 0.7). The inset shows the saturation magnetization (Ms) and coercivity (Hc) of thin films as a function of Zn substitution (x).

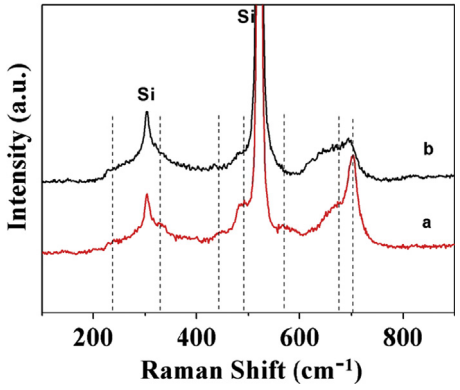

Fig. 3. Raman spectra of the NZFO thin films (a) x=0 and (b) x=0.5.

Fig. 3 shows Raman scattering data of $NiFe_2O_4$ and $Ni_{0.5}Zn_{0.5}Fe_2O_4$ thin films at room temperature. thin films. As seen from Fig. 3, the widened peaks marked with dash lines indicated that both films presented the characteristics of (Ni, Zn) Fe_2O_4 ferrite , which were also demonstrated by Chen et al. [20]. Similar Raman spectra indicated that both films presented a same crystalline structure. Comparing with NZFO film of $x=0$, a little blue shift and the decrease of relatively peak intensity were observed for the $Ni_{0.5}Zn_{0.5}Fe_2O_4$ film. Moreover, no other peaks presented in the Raman spectra, indicating no impurity phase in the specimens.

Fig. 4 is the XPS spectra of $Ni_{0.5}Zn_{0.5}Fe_2O_4$ film. As seen from the inset, the electron spectra of Zn $2p_{3/2}$ (Fig. 4a), Ni $2p_{3/2}$ (Fig. 4b), and Fe $2p_{3/2}$ (Fig. 4c) were observed at 1022.2 eV, 854.9 eV, and 710.4 eV, respectively, which were in good agreement with the reported results for bulk $NiFe_2O_4$ and $ZnFe_2O_4$ [21–24].

Fig. 5 is the surface morphology of $Ni_{0.5}Zn_{0.5}Fe_2O_4$ film fired at 650 °C. It is evident that the $Ni_{0.5}Zn_{0.5}Fe_2O_4$ film had uniform spherical grains with an average particle size of 43 nm, and no large pores on the film surface. Fig. 6 is the cross-section TEM image of the $Ni_{0.5}Zn_{0.5}Fe_2O_4$ film. It can be seen that the $Ni_{0.5}Zn_{0.5}Fe_2O_4$ film had the thickness of approximate120 nm and the average grain size of the film

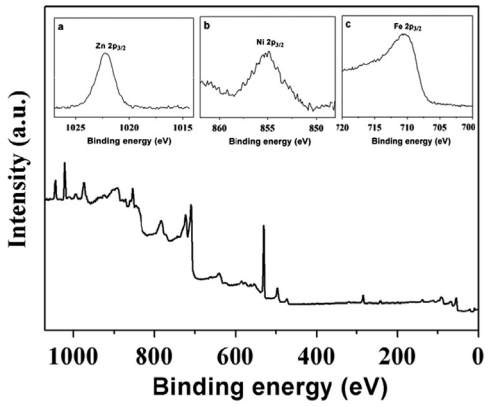

Fig. 4. XPS spectrums of the $Ni_{0.5}Zn_{0.5}Fe_2O_4$ film. The inset is the high-resolution spectra of Zn $2p_{3/2}$ (a), Ni $2p_{3/2}$ (b), and Fe $2p_{3/2}$ (c), respectively.

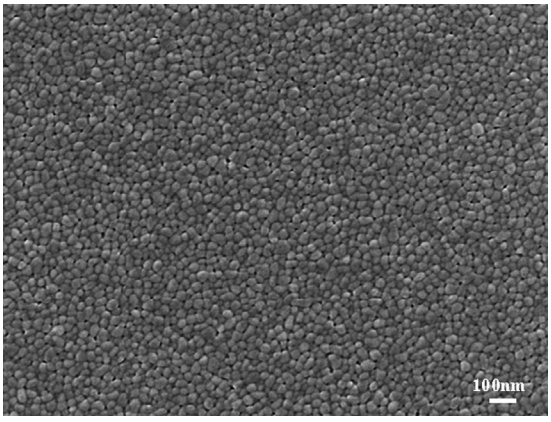

Fig. 5. The surface morphology of $Ni_{0.5}Zn_{0.5}Fe_2O_4$ film.

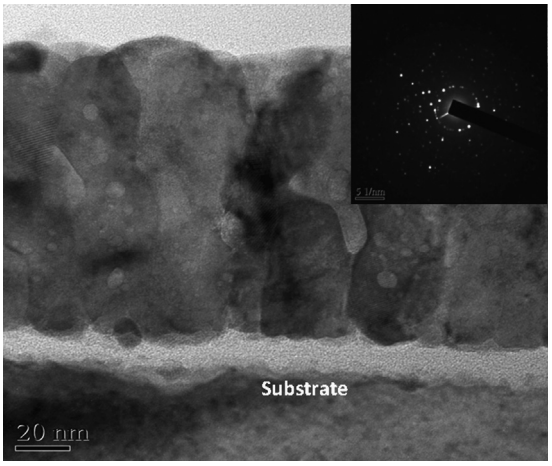

Fig. 6. Cross-section TEM micrographs for $Ni_{0.5}Zn_{0.5}Fe_2O_4$ film. The inset is the selected area electron diffraction patterns taken from the Cross-section micrographs.

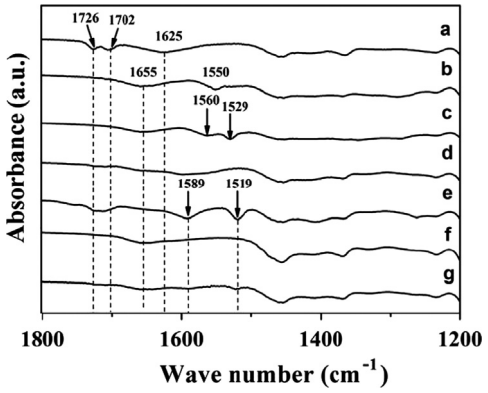

Fig. 7. FT-IR spectra of different solutions of (a) AcAcH+MOE, (b) $Fe(NO_3)_3\cdot 9H_2O$+MOE, (c) $Fe(NO_3)_3\cdot 9H_2O$+MOE+AcAcH, (d) $Ni(CH_3COO)_2\cdot 4H_2O$+MOE, (e) $Ni(CH_3COO)_2\cdot 4H_2O$+MOE+AcAcH, (f) $Zn(CH_3COO)_2\cdot 2H_2O$+MOE, (g) $Zn(CH_3COO)_2\cdot 2H_2O$+MOE+AcAcH.

about 40 nm, which agreed well with that of the surface micrograph. From the inset of the selected area electron diffraction pattern (SAED), it can further verify that the films prepared had the nanosized polycrystalline structure.

3.2. Photosensitivity and fine-patterning of the solution and gel film

Fig. 7(a–g) shows the FT-IR spectra of the gel films derived from different solutions. There were three characteristic peaks located at 1726, 1702 and 1625 cm^{-1} for the mixed solution of AcAcH and MOE, which corresponded to the $\nu_{C=O}$ mode of AcAcH (see Fig. 7(a)). After adding AcAcH into Fe-solution, two additional peaks occurred at about 1560 and 1529 cm^{-1} indicating that a chemical reaction happened between the AcAcH and the $Fe(NO_3)_3\cdot 9H_2O$. This reaction led to the formation of UV-photosensitive $Fe(AcAc)(NO)_2$ inside the gel film [25]. Similar phenomena were also found after adding AcAcH into the Ni-solution and Zn-solution (see Fig. 7(d–g)).

The UV spectra of the mixed solutions were shown from Fig. 8. As seen from Fig. 8a, a characteristic absorption peak at 272 nm was observed for AcAcH. From Fig. 8b, Fig. 8c and Fig. 8d, the absorption peaks respectively shifted to 282 nm (for Fe ion), 297 nm (for Ni ion) and 342 nm (for Zn ion) after introducing Fe, Ni and Zn into the mixed solution of AcAcH and MOE. The red shift indicated that the chelate reaction occurred between metal ions and $AcAc^-$, which can be expressed by Eq. (1), Kim et al. [26] believed that this is due to the electron transition from π to π^* during the formation process of the chelates.

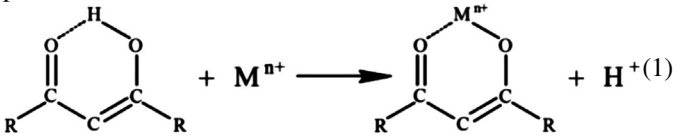

(1)

Fig. 9 is the UV–vis absorption spectra of $Ni_{0.5}Zn_{0.5}Fe_2O_4$ gel film. It is obvious that the absorption band remarkably decreased when gel films were irradiated by the UV light with a suitable wavelength. The absorption of gel films gradually decreased with prolonging UV irradiation, and finally disappeared after 15 min. This indicated the chelate decomposed during irradiating process. Hence, the intensity of the absorption band decreased with the increase of irradiation time.

It was reported that UV irradiation had a significant effect on the dissolution of gel films in appropriate organic solvents

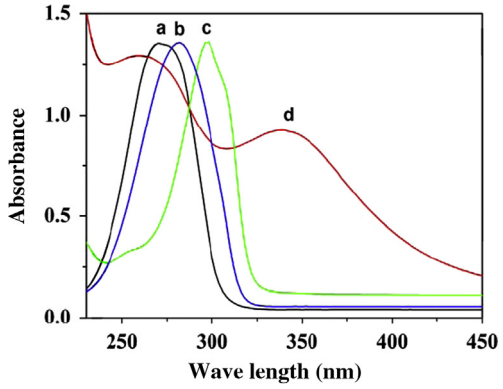

Fig. 8. UV–vis spectra of different solutions of (a) AcAcH+MOE, (b) $Fe(NO_3)_3 \cdot 9H_2O$+MOE+AcAcH, (c) $Ni(CH_3COO)_2 \cdot 4H_2O$+MOE+AcAcH, (d) $Zn(CH_3COO)_2 \cdot 2H_2O$+MOE+AcAcH.

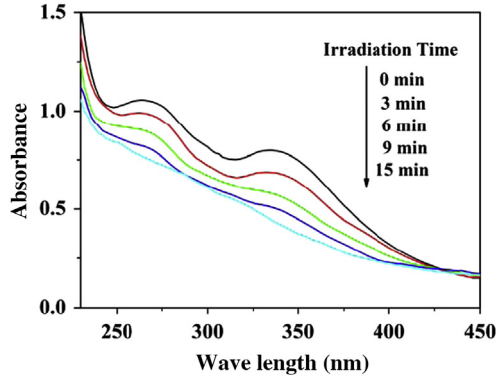

Fig. 9. UV–vis spectra of $Ni_{0.5}Zn_{0.5}Fe_2O_4$ film irradiated by UV light.

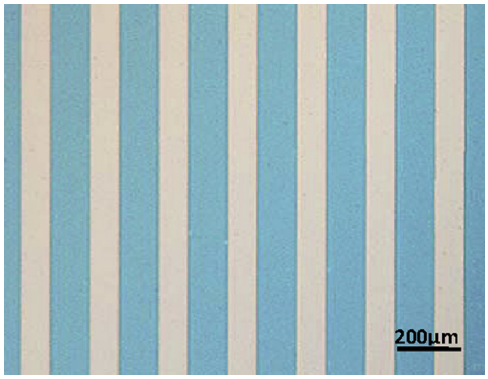

Fig. 10. Optical micrograph of an in-situ patterned $Ni_{0.5}Zn_{0.5}Fe_2O_4$ gel film.

with the decomposition of the chelates [12,25]. Fig. 10 shows the optical micrograph of an in-situ patterned $Ni_{0.5}Zn_{0.5}Fe_2O_4$ gel film. One can see that the non-irradiated part was dissolved away while the irradiated part was left, thus obtaining the fine patterns of $Ni_{0.5}Zn_{0.5}Fe_2O_4$ gel films. $Ni_{0.5}Zn_{0.5}Fe_2O_4$ gel films with the fine patterns can be further heat-treated to fabricate fine-patterned inorganic films.

4. Conclusions

Using nickel acetate, zinc acetate and ferric nitrate as starting materials, AcAcH as chelating agent, $Ni_{1-x}Zn_xFe_2O_4$ (NZFO) (x=0.0–0.7) precursor solutions were prepared. At a firing temperature of 650 °C, the films presented a nanocrystalline structure with a cubic spinel crystallography. When Ni/Zn=1, the saturation magnetization of the fired films reached the maximum value of 683 emu/cm^3 with a relative low Hc of 56 Oe. Due to the chelating reaction between AcAcH and metallic ions, the coated NZFO gel film presented photosensitivity. The fine-patterned $Ni_{0.5}Zn_{0.5}Fe_2O_4$ gel film was successfully fabricated through UV irradiation, rinsing and heat treatment.

Acknowledgments

This work is supported by the National Natural Science Foundation (Nos. 51072163, 51102195, 51001085 and 51171148).

References

[1] Q. Xie, M.H. Hong, H.L. Tan, G.X. Chen, L.P. Shi, T.C. Chong, Fabrication of nanostructures with laser interference lithography, Journal of Alloys and Compounds 449 (2008) 261–264.
[2] Y.N. Xia, G.M. Whitesides, Soft lithography, Angewandte Chemie-International Edition 37 (1998) 550–575.
[3] A. Savouchkina, A. Foelske-Schmitz, V.A. Guzenko, D. Weingarth, G.G. Scherer, A. Wokaun, R. Kötz, In situ STM study of Pt-nanodot arrays on HOPG prepared by electron-beam lithography, Electrochemistry Communications 13 (2011) 484–487.
[4] J.E.E. Baglin, Ion beam nanoscale fabrication and lithography—a review, Applied Surface Science 258 (2012) 4103–4111.
[5] S. Brose, S. Danylyuk, L. Juschkin, C. Dittberner, K. Bergmann, J. Moers, G. Panaitov, St. Trellenkamp, P. Loosen, D. Grützmacher,

Broadband transmission masks, gratings and filters for extreme ultraviolet and soft X-ray lithography, Thin Solid Films 520 (2012) 5080–5085.
[6] E.M. Park, J. Choi, B.H. Kang, K.Y. Dong, Y.K. Park, I.S. Song, B. K. Ju, Investigation of the effects of bottom anti-reflective coating on nanoscale patterns by laser interference lithography, Thin Solid Films 519 (2011) 4220–4224.
[7] H. Kim, H.H. Park, A study on the electrical properties of fluorine doped direct-patternable SnO_2 thin films, Ceramics International 38S (2012) S609–S612.
[8] S. Briche, Z. Tebby, D. Riassetto, M. Messaoud, E. Gamet, E. Pernot, H. Roussel, O. Dellea, Y. Jourlin, M. Langlet, New insights in photo-patterned sol–gel-derived TiO_2 films, Journal of Materials Science 46 (2011) 1474–1486.
[9] H.H. Park, S.B. Jung, H.H. Park, T.S. Kimb, R.H. Hill, Electrical and ferroelectric properties of SBT thin films formed by photochemical metal–organic deposition, Sensors and Actuators B 126 (2007) 289–293.
[10] Y. Chen, G. Zhao, Y. Ren, Z. Wang, Microfabrication of dilute magnetic semiconducting $Ti_{1-x}Co_xO_2$ films using photosensitive sol–gel method, Thin Solid Films 519 (2011) 1985–1988.
[11] G.Y. Zhao, H.L. Zhang, Y.Q. Chen, H.J. Peng, Fabrication of YBCO film patterns and their properties, Superconductor Science and Technology 21 (2008) 125016.
[12] Y.Q. Chen, G.Y. Zhao, F.X. Yan, Ferromagnetic Co-doped ZnO film and fine patterns prepared using photosensitive sol–gel method, Journal of Sol–Gel Science and Technology 54 (2010) 325–328.
[13] B.L. Ahuja, H.S. Mund, S. Tiwari, J. Sahariya, A. Dashora, M. Itou, Y. Sakurai, Evaluation of orbital moment in Ni–Zn ferrites: a magnetic compton scattering study, Applied Physics Letters 100 (2012) 132410.
[14] M.S. Boon, W.P.S. Saw, M. Mariatti, Magnetic, dielectric and thermal stability of Ni–Zn ferrite-epoxy composite thin films for electronic applications, Journal of Magnetism and Magnetic Materials 324 (2012) 755–760.
[15] N.H. Vasoya, L.H. Vanpariya, P.N. Sakariya, M.D. Timbadiya, T.K. Pathak, V.K. Lakhani, K.B. Modi, Synthesis of nanostructured material by mechanical milling and study on structural property modifications in $Ni_{0.5}Zn_{0.5}Fe_2O_4$, Ceramics International 36 (3) (2010) 947–954.
[16] Y.L. Liu, Y.X. Li, H.W. Zhang, D.M. Chen, C.H. Mu, Structural and magnetic properties of NiZn–ferrite thin films prepared by radio frequency magnetron sputtering, Journal of Applied Physics 109 (2011) 07A511.
[17] D.W. Guo, X.L. Fan, G.Z. Chai, C.J. Jiang, X.L. Li, D.S. Xue, Structural and magnetic properties of NiZn ferrite films with high saturation magnetization deposited by magnetron sputtering, Applied Surface Science 256 (2010) 2319–2322.
[18] K. Sun, Z.W. Lan, Z. Yu, X.L. Nie, Characterization and magnetic properties of polyethylene glycol modified NiZn ferrite thin films, Current Applied Physics 11 (2011) 472–475.
[19] J.H. Gao, Y.T. Cui, Z. Yang, The magnetic properties of $Ni_xZn_{1-x}Fe_2O_4$ films fabricated by alternative sputtering technology, Materials Science and Engineering B 110 (2004) 111–114.
[20] D.G. Chen, X.G. Tang, J.B. Wu, W. Zhang, Q.X. Liu, Y.P. Jiang, Effect of grain size on the magnetic properties of superparamagnetic $Ni_{0.5}Zn_{0.5}Fe_2O_4$ nanoparticles by co-precipitation process, Journal of Magnetism and Magnetic Materials 323 (2011) 1717–1721.
[21] M. Lenglet, A. D'Huysser, J.P. Bonelle, J. Dürr, C.K. Jörgensen, Analysis of X-ray Nickel Kb emission, XANES, XPS, Nickel 2p, and optical spectra of nickel (II) spinels and structure inference, Chemical Physics Letters 136 (1987) 478–482.
[22] M. Pineda, J.L.G. Fierro, J.M. Palacios, C. Cilleruelo, E. Garcia, J.V. Ibarra, Characterization of zinc oxide and zinc ferrite doped with Ti or Cu as sorbents for hot gas desulphurization, Applied Surface Science 119 (1997) 1–10.
[23] Y. Hayashimto, W. Sakamoto, T. Yogo, Synthesis of nickel zinc ferrite nanoparticle/organic hybrid from metalorganics, Journal of Materials Research 22 (2007) 1967–1974.
[24] Y.Q. Tao, Z.Y. Li, K.C. Zhou, Effects of debinding atmosphere on the microstructure and sintering densification of nickel ferrite, Ceramics International 39 (2013) 865–869.
[25] F.X. Yan, G.Y. Zhao, N.N. Zhao, N. Song, Y.Q. Chen, Synthesis and characterization of photochemical sol–gel derived lanthanum doped $Bi_4Ti_3O_{12}$ film and its micro-patterns, Journal of Sol–Gel Science and Technology 64 (2012) 524–529.
[26] H.R. Kim, O.H. Park, Y.K. Choi, B.S. Bae, Photobleaching of γ-glycidoxypropyltrimethoxysilane-chelated metal alkoxide gel films, Journal of Sol–Gel Science and Technology 19 (2000) 607–610.